LETTER TO THE EDITOR

Structures of the endogenous peptide- and selective non-peptide agonist-bound SSTR2 signaling complexes

Cell Research (2022) 32:785–788; https://doi.org/10.1038/s41422-022-00669-z

Dear Editor,

Somatostatin, also known as growth hormone-inhibiting hormone, is an important peptide hormone that mediates predominantly neuroendocrine inhibitory effects in the exocrine and endocrine systems.[1,2] Besides, it can also exert potent regulatory effects on cell proliferation and angiogenesis.[3] In human, somatostatin exerts its physiological functions through activating five somatostatin receptors (SSTRs), which are class A $G_{i/o}$ protein-coupled receptors. Pharmacologically, somatostatin receptors, especially SSTR2, are the primary drug targets for the treatment of pituitary adenomas and neuroendocrine tumors.[1–3] To date, three somatostatin analogs have been approved for clinical use and two of them (lanreotide and octreotide) are SSTR2-selective drugs.[3] In addition to peptidic agonists, extensive efforts have also been made to design selective small-molecule agonists,[4–7] which will facilitate the development of orally active chemotherapeutic agents. Yet, the limited structural information of SSTRs has hindered our understanding of the ligand recognition mode and the structure-guided drug discovery. Here, we present two cryo-electron microscopy (cryo-EM) structures of SSTR2–G_{i1} complexes activated by the endogenous peptide (SS-14) and a selective non-peptide agonist (L-054,264). Combined with functional analysis, our results reveal the structural basis of ligand-binding mode and non-peptide agonist subtype-selectivity of SSTR2.

To obtain stable SSTR2–G_{i1} complex, we co-expressed full-length SSTR2, the dominant-negative $G\alpha_{i1}$ ($DNG\alpha_{i1}$), $G\beta_1$ and $G\gamma_2$ in insect cells utilizing a NanoBiT tethering strategy.[8] Subsequently, the signaling complex was formed in the presence of SS-14 or L-054,264, whose activities have been confirmed by cellular signaling assays (Supplementary information, Fig. S1). The structures of SS-14- and L-054,264-bound SSTR2–G_{i1} complexes were resolved by cryo-EM to global resolutions of 2.8 Å and 2.7 Å, respectively (Supplementary information, Figs. S2, S3). The high-quality density maps allowed accurate model building for most residues of the receptor, G_{i1} and the agonists SS-14 and L-054,264, thus providing reliable models for subsequent structural analysis (Fig. 1a, b; Supplementary information, Fig. S4 and Table S1).

Globally, the SSTR2 structures adopt the canonical active-state conformations of class A peptide G-protein-coupled receptors (GPCRs),[9–11] including a similar seven-transmembrane helical (7TM) bundle, a long β-hairpin structure formed in extracellular loop 2 (ECL2), and the conserved disulfide bond between TM3 and ECL2 (Supplementary information, Fig. S5a, b). Sequence alignment and structural analysis show that the activation motifs of class A GPCR including the toggle switch, PIF, NPxxY, and DRY are present in SSTR2 and adopt classic active conformations (Supplementary information, Figs. S5c, S6), suggesting a highly conserved activation mechanism for SSTR2.[12] In addition, our structures also uncover the detailed G_{i1} coupling interface, which is composed of TM2–TM3, TM5–TM6, ICL2–ICL3 and helix 8 of the receptor and the α5-helix, β6 and β2–β3 loop of $G\alpha_{i1}$ (Supplementary information, Fig. S7). Although the overall structures of the two agonist-bound complexes are similar with an overall Cα root mean squared deviation (RMSD) of 0.68 Å, two notable differences are clearly observed (Supplementary information, Fig. S5d–f). First, compared to L-054,264-bound structure, the extracellular tips of TM7 and ECL3 in SS-14-bound structure exhibit an outward shift by 2.5 Å (measured at the Cα atoms of P288), resulting from an outward push by the bulky side chains of Phe^{6} and Phe^{11} in SS-14 (Supplementary information, Fig. S5e). Second, the orientation of G_{i1} coupling shows a slight difference between the two structures, diverging by ~4.5° (Supplementary information, Fig. S5f).

The endogenous peptide SS-14 occupies the orthosteric binding pocket comprising TM2–TM7 helices and ECL2–ECL3 (Fig. 1c–e). The conserved "W^{8}–K^{9}" motif, shared by endogenous agonists and peptide analogs (Supplementary information, Fig. S1a), inserts deeply into the 7TM and the disulfide-bonded (Cys^{3}–Cys^{14}) N- and C-terminus face the extracellular side (Fig. 1c). Detailed analysis reveals that SS-14 forms extensive polar and hydrophobic interactions with SSTR2, with a total interface area of 970 $Å^2$. In the upper part of the pocket, SS-14 mainly interacts with the ECL2, ECL3 and extracellular end of TM5–TM7, forming extensive hydrogen-bonding interactions with SSTR2, involving residues $W197^{ECL2}$, $Y205^{5.35}$, $S279^{6.58}$ and $S192^{ECL2}$ (superscripts refer to Ballesteros–Weinstein numbering[13]) (Fig. 1d; Supplementary information, Table S2). In addition to this hydrogen-bond network, the Phe^{6} of SS-14 packs against $F275^{6.54}$ and $F294^{7.35}$ to form strong π–π interactions, and the Phe^{11} makes a cation–π stacking interaction with the side chain of $K291^{7.32}$ (Fig. 1d; Supplementary information, Table S2). In the bottom of the pocket, four essential residues ($F^{7}W^{8}K^{9}T^{10}$) of SS-14 provide the main contacts with SSTR2 (450 $Å^2$, 46% of the total interface). Among them, Phe^{7} and Trp^{8} insert into two hydrophobic pockets mainly comprising residues $I195^{ECL2}$, $W197^{ECL2}$, $Y205^{5.35}$ and $I209^{5.39}$ and residues $F127^{3.37}$, $F208^{5.38}$ and $F272^{6.51}$, respectively, whereas Lys^{9} and Thr^{10} form intensive polar interactions with the residues $D122^{3.32}$, $Q126^{3.36}$, $Y302^{7.43}$, $T194^{ECL2}$ and $Q102^{2.63}$ of SSTR2 (Fig. 1e; Supplementary information, Table S2).

To correlate these structural findings with signaling profiles, we utilized site-directed mutagenesis coupled with NanoBiT G-protein dissociation assays. The majority of alanine mutations in the orthosteric peptide-binding pocket reduced the potency of SS-14 (Fig. 1f; Supplementary information, Fig. S8 and Tables S3, S6). Notably, mutation of several "key sites" strongly impaired the agonist potency, highlighting their importance in SS-14 recognition. First, mutation of $D122^{3.32}$, $Q126^{3.36}$ or $Y302^{7.43}$ to alanine, abolishing the salt bridge or hydrogen bond with Lys^{9}, decreased the agonist potency by 39-fold, 37-fold and 832-fold, respectively (Fig. 1f; Supplementary information, Fig. S8 and Tables S3, S6). Second, alanine substitution of $F127^{3.37}$, $F208^{5.38}$ and $F272^{6.51}$ that make hydrophobic contacts with Trp^{8} led to significantly decreased potency

Received: 10 January 2022 Accepted: 12 April 2022
Published online: 16 May 2022

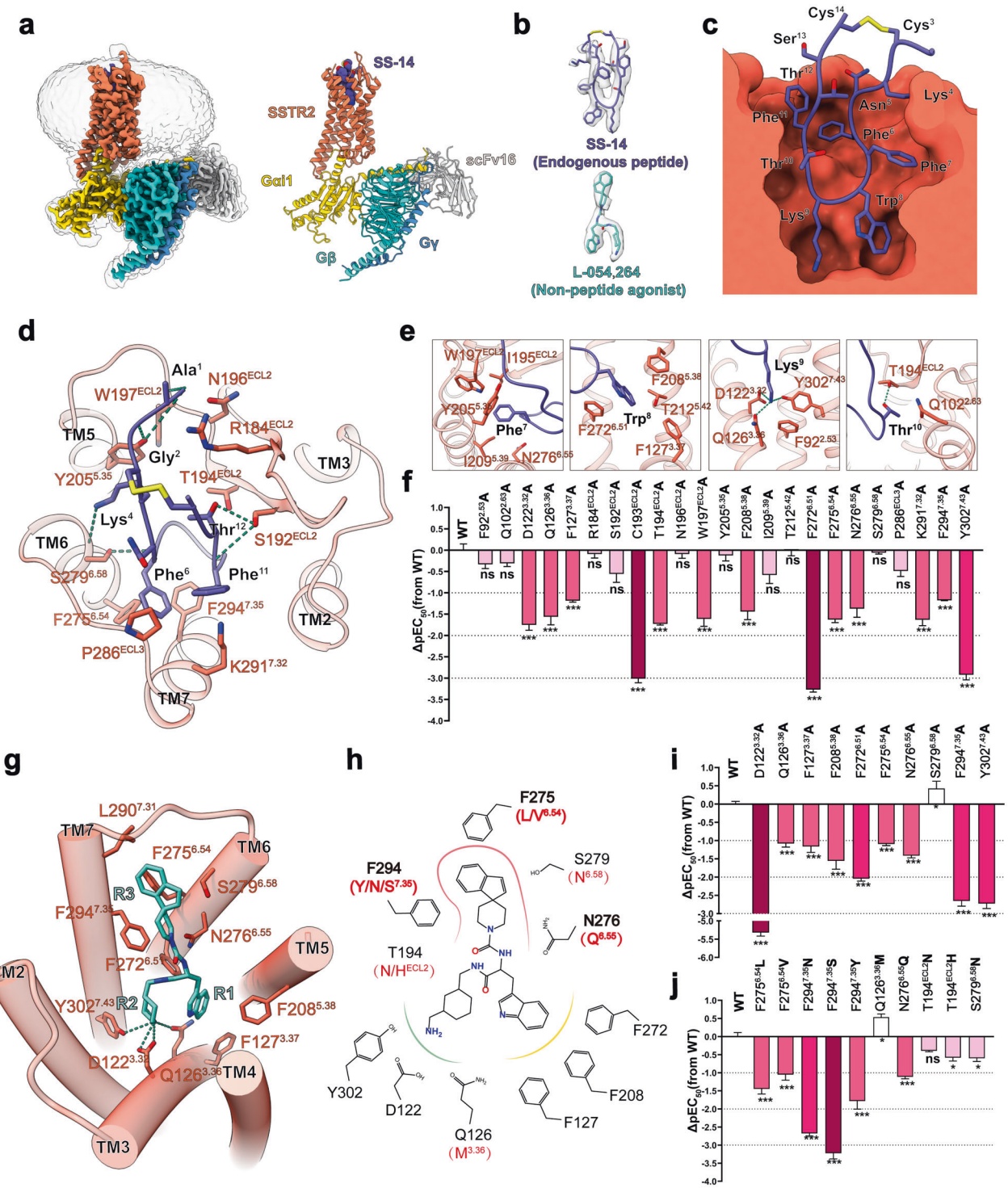

Fig. 1 Cryo-EM structures of the SSTR2–G_{i1} complexes. **a** Cryo-EM map and structural model of SS-14-bound SSTR2–G_{i1} complex. SSTR2, orange; SS-14, medium purple; $G\alpha_{i1}$, yellow; Gβ, ocean blue; Gγ, cornflower blue; scfv16, gray. **b** Cryo-EM densities and models of endogenous peptide agonist SS-14 and small-molecule agonist L-054,264 from their activated SSTR2–G_{i1} complexes, respectively. SS-14, medium purple; L-054,624, cyan; cryo-EM density is shown at 0.2 contour level. **c** Cross-section of SS-14-binding pocket in SSTR2. **d** Top view on SS-14-binding pocket highlights the hydrogen-bond network in upper part of this orthostatic pocket. **e** Detailed interactions between SSTR2 and four essential residues ($F^7W^8K^9T^{10}$) of SS-14. Hydrogen bonds and salt bridge are depicted as green dashed lines. **f** Effects of mutations in SS-14-binding pocket on SS-14-induced G_{i1} signaling. **g** Detailed interactions of small-molecule agonist L-054,264 (cyan) with SSTR2 (orange). **h** Schematic representation of the residues involved in L-054,264 recognition and subtype-selectivity. **i** Effects of mutations in L-054,264-binding pocket on L-054,264-induced G_{i1} signaling. **j** Effects of mutations of the potential residues involved in L-054,264 subtype-selectivity on G_{i1} signaling. The L-054,264-induced G_{i1} signaling was detected by NanoBiT G-protein dissociation assay. Bars represent differences in calculated agonist potency (pEC_{50}) for each mutant relative to the wild-type receptor (WT). Data are colored according to the extent of effect. $^{ns}P > 0.01$, $^{*}P < 0.01$, $^{**}P < 0.001$ and $^{***}P < 0.0001$ (one-way ANOVA followed by Dunnett's multiple comparison test, compared with the response of WT. Data are shown as means ± SEM from three independent experiments.

of SS-14 (Fig. 1f; Supplementary information, Fig. S8 and Tables S3, S6). Third, mutation of $T194^{ECL2}$ and $W197^{ECL2}$ in ECL2 or mutation of $C193^{ECL2}$ to alanine to break the conserved disulfide bond ($C115^{3.25}$–$C193^{ECL2}$) that is crucial for the conformational stability of ECL2, showed significant effects on agonist potency, revealing the important role of ECL2 in peptide ligand binding (Fig. 1f; Supplementary information, Fig. S8 and Tables S3, S6). Collectively, our structural and functional results reveal the critical roles of "W^8–K^9" dipeptide of peptide agonist in receptor activation and show that the ECL2 of SSTR2 is also crucial in peptide agonist recognition.

Currently, several SSTR2-selective non-peptide agonists have been reported such as L-054,264, L-779,976 and L-054,522.[4–6] These agonists display similar chemical scaffold (Supplementary information, Fig. S1a) and show at least 1000-fold selectivity for SSTR2[4–6] compared with other SSTRs. Here, the commercially available L-054,264 was chosen for structural determination for the analysis of non-peptide agonist binding mode and selectivity. Our structure reveals that L-054,264 adopts an inverted Y-shaped configuration, the R1 and R2 moieties insert into the bottom of the ligand-binding pocket and the R3 moiety points toward the extracellular vestibule (Fig. 1g). Compared to the peptide agonist discussed above, the conformational architecture of R1 and R2 in L-054,264 resembles the conserved W^8–K^9 pharmacophore of SS-14, while R3 occupies the corresponding place of Phe^6 in the peptide structure (Supplementary information, Fig. S9a). In general, L-054,264 shows a similar interface as the peptide agonist at the bottom of the pocket, but displays fewer interactions with ECL2 in the upper part of the pocket, resulting in a smaller interface (424 Å^2) (Fig. 1g; Supplementary information, Table S4).

The R1 moiety (indole group) of L-054,264 physicochemically equivalent to Trp^8 of SS-14, displays similar interactions with $F127^{3.37}$, $F208^{5.38}$ and $F272^{6.51}$ (Fig. 1g, h). Functional assays also showed that mutation of these residues severely reduced the L-054,264-induced receptor activation (Fig. 1i; Supplementary information, Fig. S9b and Tables S5, S6). The R2 moiety structurally mimicks the side chains of Lys^9 in SS-14 with more rigidity owing to the cyclohexane ring, and inserts less deep into the negatively charged pocket consisting of $D122^{3.32}$, $Q126^{3.36}$, and $Y302^{7.43}$ (Fig. 1g, h; Supplementary information, Fig. S9a). Interestingly, our signaling assays illustrated that $D122^{3.32}$A mutant showed more severe impairment on L-054,264 potency than that of SS-14 (> 1000 fold) (Fig. 1i; Supplementary information, Fig. S9b and Tables S5, S6), indicating the essential role of this salt bridge between $D122^{3.32}$ and the amine group of R2 in non-peptide agonist binding. Of note, the signaling assays also showed that the $D122^{3.32}$A mutant significantly decreased the efficacy for both types of agonists, indicating its critical roles in the ligand-dependent activation of SSTR2 (Supplementary information, Figs. S8b and S9b). Apart from the pivotal R1 and R2 moieties, the R3 moiety also forms extensive hydrophobic interactions with the residues at the extracellular end of TM6 and TM7. It is noteworthy that $F294^{7.35}$ makes strong hydrophobic interactions with the piperidine ring in R3 and is crucial for L-054,264 recognition, as confirmed by our mutation experiments (Fig. 1g–i; Supplementary information, Fig. S9b and Tables S5, S6).

To find out the mechanism of SSTR2-selectivity for L-054,264, homology models of other SSTRs were generated based on our determined SSTR2 structure using SWISS-MODEL.[14] Structural comparison of the agonist-binding pocket among SSTRs revealed several non-conserved residues that might make differential interaction or potential steric clash with L-054,264, including $Q126^{3.36}$, $T194^{ECL2}$, $F275^{6.54}$, $N276^{6.55}$, $S279^{6.58}$, $F294^{7.35}$ (Supplementary information, Fig. S10a–d). The majority of these residues participate in the recognition of the R3 moiety (Fig. 1h), highlighting the significance of R3 in receptor selectivity. To test our hypothesis, we replaced these residues in SSTR2 with the corresponding residues in other SSTRs and evaluated the influence of the mutations to the potency of L-054,264 using NanoBiT assay. Replacement of $F275^{6.54}$ ($L^{6.54}$ in SSTR3; $V^{6.54}$ in SSTR1, 4, 5), $F294^{7.35}$ ($S^{7.35}$ in SSTR1; $N^{7.35}$ in SSTR4; $Y^{7.35}$ in SSTR3, 5) and $N276^{6.55}$ ($Q^{6.55}$ in SSTR1, 4) with the corresponding residues in other receptors displayed significant reduction in pEC_{50} for L-054,264 (Fig. 1j; Supplementary information, Fig. S10e, f and Tables S5, S6). Notably, $F275^{6.54}$ and $F294^{7.35}$ are only present in SSTR2 and pack tightly against the piperidine and indene rings in the R3 moiety of L-054,264 (Fig. 1g, h; Supplementary information, Fig. S6). Interestingly, the unique residues in SSTR2, $F275^{6.54}$ and $F294^{7.35}$, also participate in SS-14 recognition (Fig. 1d, f), which might be an explanation for the slightly higher binding affinity of SS-14 for SSTR2.[4–6] Together, these results show that $F275^{6.54}$, $F294^{7.35}$ and $N276^{6.55}$ are key residues responsible for selective recognition of L-054,264 by SSTR2.

In conclusion, we report two cryo-EM structures of the SSTR2–G_{i1} complexes bound to the peptide and selective non-peptide agonists, which provides molecular details of agonist binding and receptor subtype-selectivity (Fig. 1). Summarizing the structural findings in combination with signaling data, we show that the two small cavities at the bottom of the ligand-binding pocket are critical for ligand binding and SSTR2 activation for both types of agonists. In addition, we also demonstrate that the ECL2 of SSTR2 contributes greatly to the binding of the peptide agonist SS-14, but plays little role in L-054,264 recognition (Fig. 1d, g). Regarding the mechanism of ligand selectivity, our structures together with mutagenesis studies reveal that the non-conserved residues $F275^{6.54}$, $F294^{7.35}$ and $N276^{6.55}$ are involved in the selective recognition of L-054,264 by SSTR2 (Fig. 1h, j). Importantly, the hydrophobic packing between the residues $F275^{6.54}$ and $F294^{7.35}$ with the R3 moiety of non-peptide agonist are critical determinants for selective recognition among SSTRs (Fig. 1h, j; Supplementary information, Fig. S6). Recently, Robertson et al.[15] reported the selective mechanism of the peptide analog, Octreotide, in *bioRxiv*. Interestingly, different from the non-peptide agonist described in this paper, the subtype-selectivity of Octreotide is more complicated and has been linked to the dynamic behavior and sequence divergence of ECL2 in SSTRs. In addition, Robertson et al. confirmed the previous finding that $F294^{7.35}$ and $N276^{6.55}$ in SSTR2 also participate in the selective recognition of Octreotide.[16] Collectively, these insights enhance the comprehensive understanding of the ligand recognition and signal transduction mechanism of the SSTRs and facilitate future structure-based drug discovery efforts, especially for selective small-molecule compounds, targeting SSTRs.

Li-Nan Chen[1,2,3,9], Wei-Wei Wang[4,9], Ying-Jun Dong[1,9], Dan-Dan Shen[1], Jia Guo[1], Xuefei Yu[5], Jiao Qin[1], Su-Yu Ji[1], Huibing Zhang[1], Qingya Shen[1], Qiaojun He[6], Bo Yang[6], Yan Zhang[1,3,4,7,8], Qinglin Li[5]✉ and Chunyou Mao[2,3]✉

[1]*Department of Biophysics and Department of Pathology of Sir Run Run Shaw Hospital, Zhejiang University, School of Medicine, Hangzhou, Zhejiang, China.* [2]*Department of General Surgery, Sir Run Run Shaw Hospital, Zhejiang University School of Medicine, Hangzhou, Zhejiang, China.* [3]*Center for Structural Pharmacology and Therapeutics Development, Sir Run Run Shaw Hospital, Zhejiang University School of Medicine, Hangzhou, Zhejiang, China.* [4]*Liangzhu Laboratory, Zhejiang University Medical Center, Hangzhou, Zhejiang, China.* [5]*The Cancer Hospital of the University of Chinese Academy of Sciences (Zhejiang Cancer Hospital), Hangzhou, Zhejiang, China.* [6]*Zhejiang Province Key Laboratory of Anti-Cancer Drug Research, College of Pharmaceutical Sciences, Zhejiang University, Hangzhou, Zhejiang, China.* [7]*MOE Frontier Science Center for Brain Research and Brain-Machine Integration, Zhejiang University School of Medicine, Hangzhou, Zhejiang, China.* [8]*Zhejiang Provincial Key Laboratory of Immunity and Inflammatory diseases, Hangzhou, Zhejiang, China.* [9]*These authors contributed equally: Li-Nan Chen, Wei-Wei Wang, Ying-Jun Dong.* ✉*email: qinglin200886@126.com; maochunyou@zju.edu.cn*

DATA AVAILABILITY

The atomic coordinates and the electron microscopy maps of SS-14- and L-054,264-bound SSTR2–G_{i1} complexes have been deposited in the Protein Data Bank (PDB) under accession numbers 7WIC, 7WIG and Electron Microscopy Data Bank (EMDB) under accession codes EMD-32528, EMD-32529, respectively.

REFERENCES

1. Weckbecker, G. et al. *Nat. Rev. Drug Discov.* **2**, 999–1017 (2003).
2. Gunther, T. et al. *Pharmacol. Rev.* **70**, 763–835 (2018).
3. Theodoropoulou, M. & Stalla, G. K. *Front. Neuroendocrinol.* **34**, 228–252 (2013).
4. Yang, L, et al. *J. Med. Chem.* **41**, 2175-2179 (1998).
5. Rohrer, S. P. et al. *Science* **282**, 737–740 (1998).
6. Yang, L. et al. *Proc. Natl. Acad. Sci. USA* **95**, 10836–10841 (1998).
7. Berk, S. C. et al. *J. Comb. Chem.* **1**, 388–396 (1999).
8. Duan, J. et al. *Nat. Commun.* **11**, 4121 (2020).
9. Harris, J. A. et al. *Nat. Chem. Biol.* **18**, 109–115 (2021).
10. Yin, Y. L. et al. *Nat. Struct. Mol. Biol.* **28**, 755–761 (2021).
11. Zhou, F. et al. *Cell Res.* **31**, 929–931 (2021).
12. Zhou, Q. et al. *Elife* **8**, e50279 (2019).
13. Ballesteros, J. A. & Weinstein, H. in Methods in Neurosciences Vol. 25. Stuart C. Sealfon ed. Academic Press. 366–428 (1995).
14. Waterhouse, A. et al. *Nucleic Acids Res.* **46**, W296–W303 (2018).
15. Robertson, M. J., Meyerowitz, J. G., Panova, O., Borrelli, K. & Skiniotis, G. *bioRxiv* https://doi.org/10.1101/2021.11.02.466988 (2021).
16. Liapakis, G. et al. *J. Biol. Chem.* **271**, 20331–20339 (1996).

ACKNOWLEDGEMENTS

The cryo-EM data were collected at the Cryo-Electron Microscopy Center, Zhejiang University. Protein purification was performed at the Protein Facilities, Zhejiang University School of Medicine. This project was supported by the National Natural Science Foundation of China (81922071 to Y.Z. and 32100959 to C.M.), Zhejiang Province Natural Science Fund for Excellent Young Scholars (LR19H31000 to Y.Z. and LR22C050002 to C.M.), the Ministry of Science and Technology (2019YFA050880 to Y. Z.), and the Key R&D Projects of Zhejiang Province (2021C03039 to Y.Z.).

AUTHOR CONTRIBUTIONS

Y.Z. and C.M. conceived and supervised the whole project; C.M. purified the SSTR2–G_{i1} complexes; D.-D.S. evaluated the sample by negative-stain EM; S.-Y.J. prepared the cryo-EM grids; J.G. and J.Q. collected the cryo-EM data; L.-N.C. performed cryo-EM map calculation and model building; L.-N.C. and Y.-J.D. generated the constructs of mutants; L.-N.C., W.-W.W., X.Y. and Q.L. performed the cellular functional assays; L.-N.C. and Y.-J.D. prepared the figures; Q.S., H.Z., Q.H. and B.Y. participated in data analysis. Q.L. edited the manuscript. C.M. and Y.Z. wrote the manuscript with inputs from all the authors.

COMPETING INTERESTS

The authors declare no competing interests.

ADDITIONAL INFORMATION

Supplementary information The online version contains supplementary material available at https://doi.org/10.1038/s41422-022-00669-z.

Correspondence and requests for materials should be addressed to Qinglin Li or Chunyou Mao.

Reprints and permission information is available at http://www.nature.com/reprints